2009 IEEE/ASME International Conference on Advanced Intelligent Mechatronics
Suntec Convention and Exhibition Center
Singapore, July 14-17, 2009

# High-speed Vertical Positioning for Contact-mode Atomic Force Microscopy

Andrew J. Fleming

*Abstract*— **Many popular modes of scanning probe microscopy require a vertical feedback system to regulate the tip-sample interaction. Unfortunately the vertical feedback controller imposes a severe limit on the scan-speed of scanning probe microscopes. In this paper, the foremost bandwidth limitation is identified to be the low-frequency mechanical resonances of the scanner. To overcome this limitation, a dual-stage vertical positioner is proposed. In this work, the bandwidth of a contact-mode atomic force microscope is increased from 83 Hz to 2.7 kHz. This improvement allows image quality to be retained with a speed increase of 33 times, or alternatively, feedback error can be reduced by 33 times if scan speed is not increased.**

## I. Introduction

The fundamental operation of an SPM is to scan a probe over a surface and map the interactions that occur as a function of location. In addition to topographic imaging, SPM probes have diversified to allow the mapping of a wide range of electrical, mechanical, chemical, biological and physical interactions [1]–[5].

There are three main limitations to the speed of a scanning probe microscope [6]: 1) The resonance frequency or bandwidth of the probe [7]; 2) The mechanical bandwidth of the scanner [6], [8]–[10]; and 3) The bandwidth of the vertical feedback system [6], [8]. These limitations have motivated extensive research on the design and control of scanning probe microscopes. Recent reviews of this research can be found in references [11], [6] and [12].

Many different techniques have been proposed to address point 1). These include self actuating cantilevers [13], active cantilever Q control [14], and short, high-speed cantilevers with resonance frequencies over 1 MHz [6], [15]. In recent years, considerable improvements have also been made to the mechanical bandwidth of the scanner [9], [10]. The greatest speed increases have resulted from completely new mechanical designs, such as [6], [8], [16]–[19]. Alternatively, more moderate but still substantial speed increases have also been achieved by better control of existing hardware. Such techniques include: actuator linearization [9], [20], [21], feedforward control and input shaping [9], [22], and improved feedback control [6], [8]–[10].

The final remaining speed limitation of a scanning probe microscope is the vertical feedback bandwidth [6], [8], [11], [12]. That is, the bandwidth of the control loop that maintains a constant force interaction between the probe and sample. This topic is discussed in detail in Section III. Although some imaging modes do not require vertical feedback, for example constant-height mode, these are used only in applications where the sample is extremely flat and immune to probe damage.

School of Electrical Engineering and Computer Sceince, University of Newcastle, Callaghan, NSW 2308, Austalia. Email: andrew.fleming@newcastle.edu.au

This research was supported by the Australian Research Council (DP0666620) and the Centre for Complex Dynamic Systems and Control. Experiments were conducted at the Laboratory for Dynamics and Control of Nanosystems, University of Newcastle.

As the main bandwidth limitation of the vertical feedback loop is due to scanner resonance, a number of approaches have been proposed that either improve the resonance frequency of the scanner or eliminate it from the feedback loop. All of the high-speed microscope designs incorporate scanners with high vertical resonance frequencies, typically above 100 kHz [8], [16]–[18], [23]. Other designs, that eliminate scanner dynamics from the feedback loop, include piezoelectric actuated probes [24], magnetically actuated probes [25], and electrostatically actuated probes [26].

Although all of these techniques are effective in their own right, none have become widely used in commercial microscopes; presumably because they require highly specialized probes and/or significant mechanical modifications. None can be applied directly to a standard scanning probe microscope without significant modification.

In this work, a new technique is described for improving the bandwidth of the vertical feedback control system. A small auxiliary positioning device with high resonance frequency is used in a dual-stage configuration with the microscope's standard positioner. Resonance frequency is increased from 680 Hz to 23 kHz, which allows an increase in bandwidth from 83 Hz to 2.7 kHz. This results in a significant image quality improvement, particularly when scanning at large range or high speed. The auxiliary system is mechanically and electrically simple and can be retrofitted to practically any present or past scanning probe microscope.

## II. Experimental Setup

In this work, an NT-MDT Ntegra scanning probe microscope is used to demonstrate the proposed techniques. The scanner is an NT-MDT piezoelectric tube scanner with 100-$\mu$m lateral range and 10-$\mu$m vertical range. The scanner comprises two piezoelectric tubes joined at the base. One tube is used for lateral positioning, and the other for vertical positioning. The internal and external electrodes of the vertical positioner are driven with equal but opposite voltages.

A signal access module allows direct access to the cantilever deflection, scanner electrode voltages, and reference trajectory.

## III. Vertical Feedback Dynamics

The vertical feedback control system for an atomic force microscope is pictured in Figure 1(a). This microscope is operating in constant-force contact-mode. The piezoelectric tube scanner moves the probe in a vertical direction to regulate the cantilever deflection $dfl$ to the set-point $r$. The cantilever deflection is measured in the standard way using a reflected laser beam and photodiode [12].

Although the diagram in Figure 1(a) represents an AFM operating in constant-force contact-mode, the schematic is similar to all forms of SPM where the tip-sample interaction is controlled. The only difference between operating modes is the measured feedback variable. For example, in contact-mode AFM, the feedback variable is cantilever deflection, while in STM, the feedback variable is tunneling current.

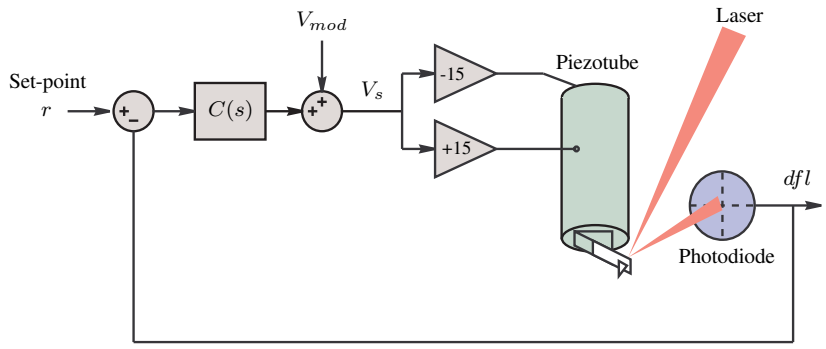


(a) Standard vertical feedback control loop

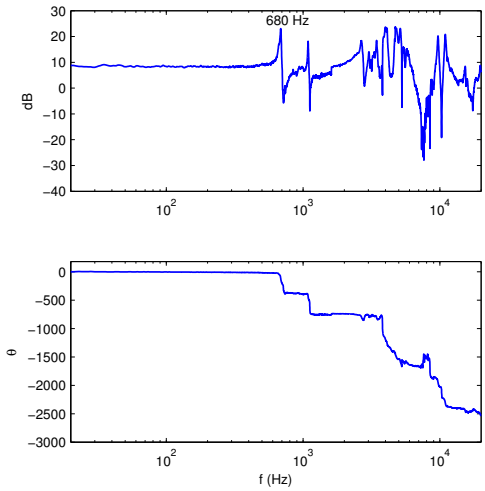


(b) Frequency response of the standard vertical positioning system $G_{dV_s}$ measured from the applied voltage $V_s$ to the cantilever deflection $dfl$

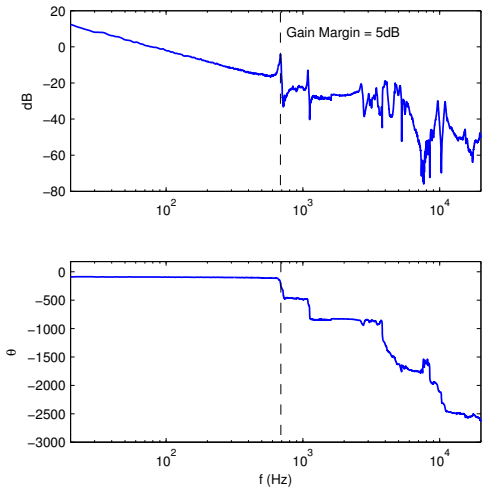


(c) Loop gain of the vertical feedback loop with an integral controller of gain $\alpha$=190. The closed-loop bandwidth is 83 Hz.

Fig. 1. **Standard vertical feedback control system**. (a) Schematic Diagram, (b) open-loop frequency response and (c) loop-gain.

Other feedback variables include the cantilever oscillation magnitude in tapping-mode AFM and the fiber oscillation magnitude in scanning near-field optical microscopy. All of these modes share the same feedback system but with different feedback variables or methods of detection.

The vertical feedback control system in Figure 1(a) comprises the set-point summing junction, the controller $C(s)$ and the driving amplifiers, which in this case are connected to the internal and external tube electrodes. The controller $C(s)$ is most commonly an integral controller, i.e.,

$$C(s) = \frac{\alpha}{s} \tag{1}$$

Integral controllers are popular as they are simple to implement, provide good regulation of tip-sample interaction at low frequencies, and are easily adjustable. Ease of tuning is a necessity as the feedback system must accommodate multiple SPM modes and cope with a wide range of probes and samples.

From a control perspective, the plant under consideration consists of all dynamics between the control voltage $V_s$ and the measured deflection $dfl$. This encompasses the amplifier dynamics, the scanner and cantilever mechanics and the tip-sample interaction. This system is denoted $G_{dV_s}$, where

$$G_{dV_s}(s) = \frac{dfl(s)}{V_s}. \tag{2}$$

Although the system $G_{dV_s}$ cannot be measured in open-loop, it is straight-forward to do so in closed-loop. This is achieved by first approaching the probe to the sample, then drastically reducing the gain of the integral controller $\alpha$ until the controller only maintains the correct DC operating point. The dynamic frequency response of $G_{dV_s}$ can then be measured directly by applying an excitation to $V_{mod}$. The experimental response of $G_{dV_s}$ is plotted in Figure 1(b). The response is essentially flat from DC to 680 Hz where the first resonance frequency of the scanner occurs. The resonance at 680 Hz is the first lateral bending mode of the scanner coupled into the vertical response. Following is the second lateral bending mode, then a dense collection of modes including torsional modes and the first piston mode [27].

From the frequency response in Figure 1(b) it is clear that $G_{dV_s}$ is an extremely complicated system. It contains the mechanical scanner dynamics, the tip-sample interaction and the dynamics of the driving and sensing electronics. However, from a control perspective, there are essentially

only two important features: the DC sensitivity $G_{dV_s}(0)$ and the first resonance mode.

The DC sensitivity is a function of the amplifier gain, scanner sensitivity, cantilever geometry, sample stiffness, and detector sensitivity. All of these are constants except for the cantilever geometry and sample stiffness, which can vary widely. The variation in these parameters is the foremost reason that vertical feedback controllers must be retuned whenever a significant change in the cantilever or sample is made.

While the DC sensitivity of $G_{dV_s}$ is a function of many microscope properties, the dynamic characteristics of $G_{dV_s}$ are clearly dominated by the scanner mechanics. Although the tip-sample interaction and cantilever dynamics are also important, these occur at much higher frequencies than the first scanner resonance and have little effect on the control performance. Instead, the maximum controller gain and closed-loop bandwidth are dependent on the resonance frequency and damping ratio of the first resonant mode. This can be understood by considering the frequency response of the controller loop-gain $C(s) \times G_{dV_s}(s)$ plotted in Figure 1(c).

From the plot of loop-gain in Figure 1(c), it is clear that the controller gain is limited by the low gain-margin imposed by the first mechanical resonance at 680 Hz. Due to the large phase drop at this frequency, the loop-gain must be less than 0 dB if the system is to be stable. The condition when this occurs is

$$P\ G_{dV_s}(0)\ \frac{\alpha}{\omega_1} < 1, \tag{3}$$

where $P$ is the difference between the DC sensitivity $G_{dV_s}(0)$ and the peak magnitude of the first resonance mode and $\omega_1$ is the first resonance frequency. $P$ is easily measured in decibels from the magnitude frequency response. In Figure 1(b), $P$ is approximately 15 dB or 5.6. Note: If $P$ is measured in dB, the value of $P$ must be converted to linear magnitude.

Rather than simply a condition on stability, it is preferable to procure a condition that guarantees a certain amount of gain-margin, i.e. the additional gain that can be added to the loop before the system becomes unstable. This figure is commonly chosen to be 2, or equivalently 6 dB. With the inclusion of gain-margin in the expression for maximum loop-gain, equation (3) becomes

$$P\ G_{dV_s}(0)\ \frac{\alpha}{\omega_1} < \frac{1}{\text{gain-margin}}, \tag{4}$$

where gain-margin should be expressed as a linear quantity.

From the expression of maximum loop-gain in equation (4), the maximum controller gain $\alpha_{\max}$ can be derived,

$$\alpha_{\max} < \frac{\omega_1}{P\ G_{dV_s}(0)} \times \frac{1}{\text{gain-margin}}. \tag{5}$$

That is, the controller gain can be increased if the first resonance frequency $\omega_1$ is increased or the magnitude of the resonance peak is decreased.

With an integral controller, the closed-loop transfer function can be approximated by

$$G_{cl}(s) = \frac{\alpha G_{dV_s}(0)}{s + \alpha G_{dV_s}(0)}. \tag{6}$$

The maximum closed-loop bandwidth of this system is approximately $\alpha_{\max} G_{dV_s}(0)$. If the expression for maximum controller gain (5) is substituted, the maximum closed-loop bandwidth can be found as a function of only the resonance frequency, peak magnitude and desired gain-margin,

$$\text{max. bandwidth} = \frac{\omega_1}{P} \times \frac{1}{\text{gain-margin}}, \tag{7}$$

thus, the maximum closed-loop bandwidth increases as the first resonance frequency $\omega_1$ is increased or the magnitude of the resonance peak is decreased.

Considering the open-loop frequency response in Figure 1(b) and equation (7), the maximum closed-loop bandwidth should be approximately 680/5.6 = 120 Hz. With a gain-margin of 5 dB the estimated closed-loop bandwidth decreases to 68 Hz. This compares well to the experimental closed-loop bandwidth of 83 Hz. This value was determined from the closed-loop frequency response plotted in Figure 4. The controller gain was $\alpha$=190, which resulted in a gain-margin of 5 dB. The discrepancy between the estimated and measured closed-loop bandwidth is due to the large tolerance in capacitive components used to implement the analog controller.

The imaging consequences of the low vertical feedback bandwidth are discussed in Section VI.

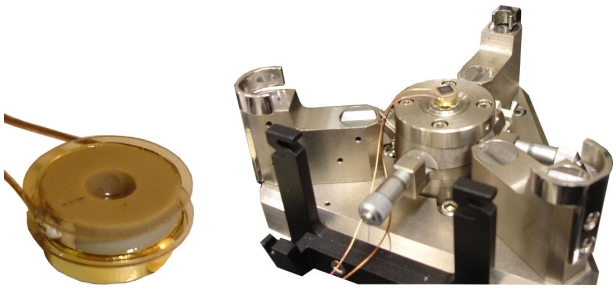

(a) (b)

Fig. 2. High-speed vertical positioner (a), mounted on the microscope base with an attached sample (b).

## IV. High-speed Vertical Positioning

From the previous section, and in particular, from equation (7), it should be clear that the frequency of the first mechanical resonance determines the maximum closed-loop bandwidth of the vertical feedback system. Hence, to improve the closed-loop response, the first resonance frequency of the scanner must be increased.

With a tube scanner, the only practical method of increasing the resonance frequency is to reduce the tube dimensions. However, the maximum lateral deflection is also proportional to the length squared [28], so any increase in resonance frequency is accompanied by a proportional decrease in scan range, which is highly undesirable.

In addition to the detrimental trade-off with scan range, it is also undesirable to modify the tube as this may require significant hardware modifications. These modifications may be difficult to implement, particularly in scan-by-probe systems where the scanner is tightly integrated with the optical and probe assemblies.

A better option than modifying the tube scanner is to replace or augment the vertical positioning function with a secondary positioner. The secondary positioner should be straight-forward to integrate into a new or existing microscope when high-performance vertical feedback is required. Such a device is described in the following.

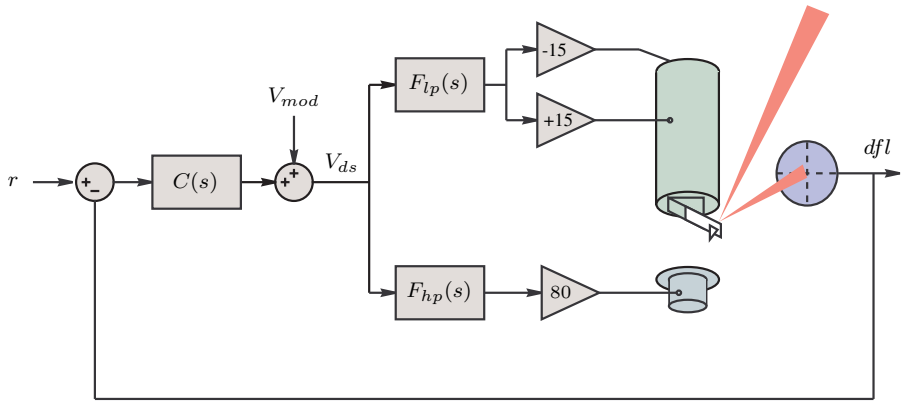


(a) Dual-stage control loop

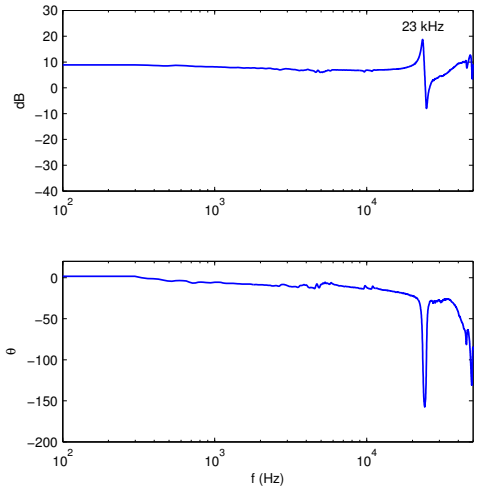


(b) Frequency response of the dual-stage positioning stage $G_{ds}$ measured from the dual-stage voltage $V_{ds}$ to the cantilever deflection $dfl$

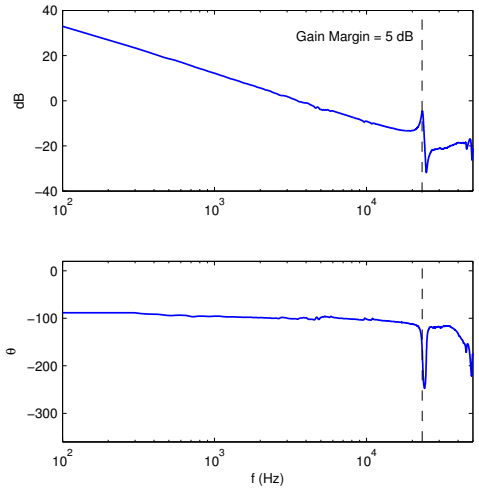


(c) Loop gain of the dual-stage vertical feedback loop with an integral controller of gain $\alpha$=10000. The closed-loop bandwidth is 2.7 kHz

Fig. 3. **Dual-stage vertical feedback control system**. (a) Schematic Diagram, (b) open-loop frequency response and (c) loop-gain.

The high-speed positioner pictured in Figure 2 comprises a piezoelectric actuator and small magnet that is highly attracted to the microscope's magnetic base. A mica wafer is used for electrical isolation between the actuator and magnet, and also as a sample substrate. The piezoelectric actuator is an 8-mm diameter multi-layer piezoelectric disk (CMAR02) manufactured by Noliac A/S, Denmark.

The piezoelectric actuator is specified to develop a stroke of 2.7 $\mu$m at 200 V. However, as the base of the actuator is constrained, the stroke when bonded to the magnet reduces to approximately 1 $\mu$m. The resonance frequency of the high-speed positioner is 23 kHz, 33 times faster than the piezoelectric tube actuator. However, the penalty is a ten-fold reduction in range.

Although a 1-$\mu$m stroke is sufficient for most forms of scanning probe microscopy, it requires an approach mechanism with extremely fine resolution. In addition, larger samples or tilted samples may also require a greater stroke, up to a few microns in some cases. To alleviate the problem of low stroke, a dual-stage approach is described in the following section that achieves both wide range and fast response.

## V. Dual-stage positioning

To facilitate probe landing and to compensate for thermal drift, a vertical positioning stroke of around 10 $\mu$m is required in general purpose microscopes. As the high-speed stage in the previous subsection only develops a 1-$\mu$m stroke, additional stroke is required from the tube scanner. The combined use of the high-speed positioner and piezoelectric tube is commonly referred to as a *dual-stage* actuator. The high-speed stage provides fast, short-range motions for imaging while the tube provides slower, long-range positioning for drift compensation and probe landing. This arrangement is illustrated in Figure 3(a).

Although there are many techniques available for the control of dual stage systems [29], only a small subset are suitable in this application. Here, simplicity is a major consideration as the system must be easily retuned (with a single parameter) for different probe and sample combinations. In addition, simplicity is also required for analog implementation which is demanded by the bandwidth and noise requirements of the control-loop.

With these considerations in mind, one option is to simply utilize the two actuators in different frequency ranges. In Fig-

**(a) Force tracking transfer function (dB versus Hz) and tracking bandwidth**

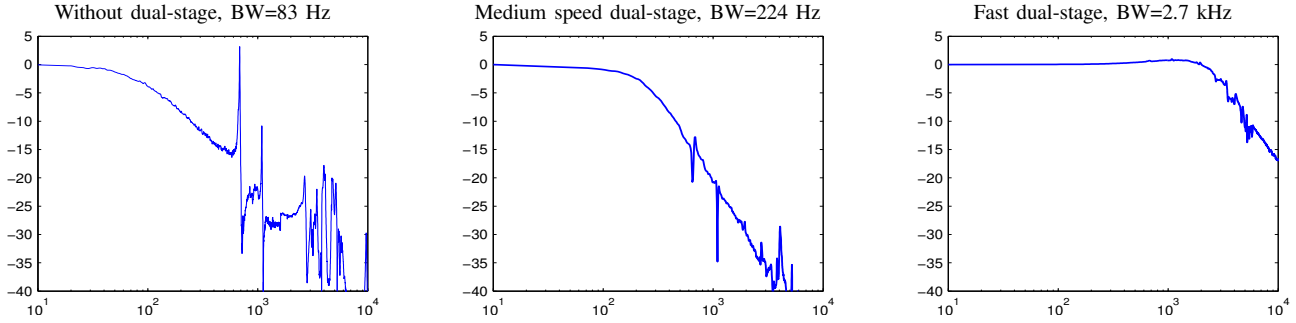


**(b) 25×25$\mu$m constant force images of a 20-nm feature height calibration standard, taken at 142 $\mu$m/s**

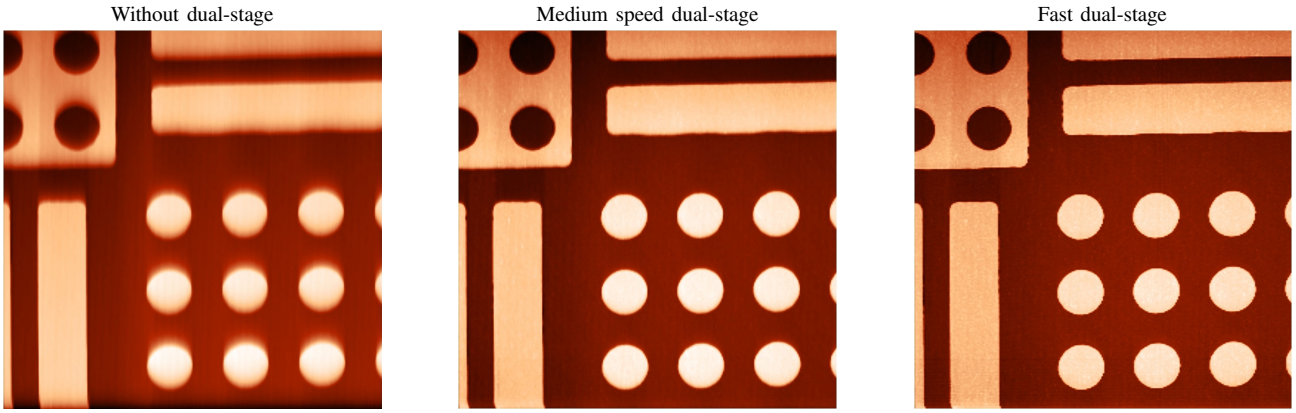


Fig. 4. Performance comparison of a standard vertical feedback controller and dual-stage controller with medium and high gain. The images were recorded at 2.84 Lines/s or 142 $\mu$m/s.

ure 3(a) a pair of complementary high- and low-pass filters $F_{hp}$ and $F_{lp}$ are shown. As these filters are complementary, they sum to 1, i.e.

$$F_{hp} + F_{lp} = 1. \tag{8}$$

A pair of complementary filters that are easy to implement with an analog circuit are,

$$F_{hp} = \frac{s}{s+\omega_c} \text{ and } F_{lp} = \frac{\omega_c}{s+\omega_c}, \tag{9}$$

where $\omega_c$ is the cut-off frequency.

With the complementary filters installed, the dual-stage transfer function from the control voltage $V_{ds}$ to the deflection $dfl$, denoted $G_{ds}$, can be expressed as the sum of the slow and fast systems $G_{dV_s}$ and $G_{dV_f}$ respectively,

$$G_{ds} = \frac{dfl}{V_{ds}} \tag{10}$$

$$= kF_{hp}G_{dV_f} + F_{lp}G_{dV_s}, \tag{11}$$

where $k$ is the gain required to equate the sensitivity of $G_{dV_f}$ to $G_{dV_s}$, i.e.

$$k = \frac{G_{dV_s}(0)}{G_{dV_f}(0)}. \tag{12}$$

In Figure 3(a) a gain of $k$=4 has been incorporated into the amplifier of the high-speed stage.

By setting the cut-off frequency $\omega_c$ one decade lower than the lowest resonance frequency of the piezoelectric tube, i.e. $\omega_c$=2$\pi$50, the product $F_{lp}G_{dV_s}$ can be approximated by $F_{lp}G_{dV_s}(0)$. Hence, the dual-stage transfer function $G_{ds}$ can also be approximated by

$$G_{ds} = kF_{hp}G_{dV_f} + F_{lp}G_{dV_s}(0) \tag{13}$$

$$= k\left(F_{hp} + F_{lp}\right)G_{dV_f} \tag{14}$$

$$= kG_{dV_f}. \tag{15}$$

That is, the dual-stage transfer function has the sensitivity of the long-range piezoelectric tube and the bandwidth of the high-speed stage. The frequency response of this transfer function is plotted in Figure 3(b).

Due to the wide bandwidth of the dual-stage system, an integral controller with a gain of $\alpha$=10000 can be applied directly while maintaining a gain-margin of 5 dB. The loop-gain with such a controller is plotted in Figure 3(c). The improvement in closed-loop bandwidth and the corresponding imaging improvements are discussed in the following section.

## VI. Imaging Experiments

In this section, the imaging performance of the dual-stage system is compared to the standard feedback system described in Section III. Due to a resonance at 680 Hz, the standard feedback system is limited to a gain of $\alpha$=190 which results in a closed-loop bandwidth of only 83 Hz. This will be compared to two dual-stage controllers, one with an intermediate gain of $\alpha$=1000, and another with the maximum gain of $\alpha$=10000.

The closed-loop frequency response, from $r$ to $dfl$, is plotted in Figure 4(a). Clearly the dual-stage controllers

provide a much wider and more regulated bandwidth. The maximum dual-stage bandwidth of 2.7 kHz is 33 times faster than the standard control system.

The effect of the improved bandwidth is demonstrated in Figure 4(b) where a BudgetSensors HS-20MG calibration standard is imaged with an NT-MDT NSG03 cantilever (90 kHz, 0.5 N/m). The lower bandwidth controller 'smears' the edges of the sample and filters small features that generate interactions above the controller bandwidth.

In addition to improving the image quality, dual-stage control can also be used for increasing the imaging speed. However, with an integral controller, as speed is increased, the force error will increase proportionally. This trade-off is summarized approximately below,

$$\text{Speed increase} \times \text{Force error reduction} = 33. \qquad (16)$$

where 33 is the factor by which the bandwidth is increased and the other variables are the factors by which speed and force error are reduced or increased. That is, if the imaging speed is kept constant, the dual-stage controller allows a reduction of force error by 33 times. Conversely, if force error is constant, the dual-stage controller allows a 33 times improvement in imaging speed.

## VII. Conclusions

The piezoelectric tubes found in a scanning probe microscope have low resonance frequencies that severely limit the vertical feedback controller bandwidth. This imposes a strict limit on maximum imaging speed if large contact forces are to be avoided.

In this work, the vertical resonance frequency is vastly improved by retro-fitting a simple high-speed dual-stage piezoelectric positioner. Thanks to the increased resonance frequency, the dual-stage configuration allowed a 33 times increase in controller gain and closed-loop bandwidth. This translates to an image quality (force error) improvement of 33 times, or a speed increase of 33 times. Visually, the dual-stage controller eliminates image smearing and faithfully reproduces fine sample features that would otherwise be lost or distorted.

## References


[1] M. J. Brukman and D. A. Bonnell, "Probing physical properties at the nanoscale," *Physics Today*, vol. 61, no. 6, pp. 36–42, June 2008.

[2] Y. F. Dufrêne, "Towards nanomicrobiology using atomic force microscopy," *Nature Reviews Microbiology*, vol. 6, pp. 674–680, September 2008.

[3] N. Jalili and K. Laxminarayana, "A review of atomic force microscopy imaging systems: application to molecular metrology and biological sciences," *Mechatronics*, vol. 14, no. 8, pp. 907–945, October 2004.

[4] E. Meyer, H. J. Hug, and R. Bennewitz, *Scanning probe microscopy. The lab on a tip*. Heidelberg, Germany: Springer-Verlag, 2004.

[5] B. Bhushan and H. Fuchs, Eds., *Applied Scanning Probe Methods (I-X)*. Heidelberg, Germany: Springer-Verlag, 2006.

[6] T. Ando, T. Uchihashi, and T. Fukuma, "High-speed atomic force microscopy for nano-visualization of dynamic biomolecular processes," *Progress in Surface Science*, vol. 83, no. 7-9, pp. 337–437, November 2008.

[7] T. Sulchek, G. G. Yaralioglu, C. F. Quate, and S. C. Minne, "Characterization and optimization of scan speed for tapping-mode atomic force microscopy," *Review of Scientific Instruments*, vol. 73, no. 8, pp. 2928–2936, 2002.

[8] G. Schitter, K. J. Åström, B. E. DeMartini, P. J. Thurner, K. L. Turner, and P. K. Hansma, "Design and modeling of a high-speed AFM-scanner," *IEEE Transactions on Control Systems Technology*, vol. 15, no. 5, pp. 906–915, September 2007.

[9] S. Devasia, E. Eleftheriou, and S. O. R. Moheimani, "A survey of control issues in nanopositioning," *IEEE Transactions on Control Systems Technology*, vol. 15, no. 5, pp. 802–823, September 2007.

[10] S. O. R. Moheimani, "Accurate and fast nanopositioning with piezoelectric tube scanners: Emerging trends and future challenges," *Review of Scientific Instruments*, vol. 79, no. 7, pp. 071 101(1–11), July 2008.

[11] D. Y. Abramovitch, S. B. Andersson, L. Y. Pao, and G. Schitter, "A tutorial on the mechanisms, dynamics, and control of atomic force microscopes," in *Proc. American Control Conference*, New York City, NY, July 2007, pp. 3488–3502.

[12] S. M. Salapaka and M. V. Salapaka, "Scanning probe microscopy," *IEEE Control Systems Magazine*, vol. 28, no. 2, pp. 65–83, April 2008.

[13] B. Rogers, T. Sulchek, K. Murray, D. York, M. Jones, L. Manning, S. Malekos, B. Beneschott, J. D. Adams, H. Cavazos, and S. C. Minne, "High speed tapping mode atomic force microscopy in liquid using an insulated piezoelectric cantilever," *Review of Scientific Instruments*, vol. 74, no. 11, pp. 4683–4686, 2003.

[14] T. Sulchek, R. Hsieh, J. D. Adams, G. G. Yaralioglu, S. C. Minne, C. F. Quate, J. P. Cleveland, A. Atalar, and D. M. Adderton, "High-speed tapping mode imaging with active q control for atomic force microscopy," *Applied Physics Letters*, vol. 76, no. 11, pp. 1473–1475, 2000.

[15] D. A. Walters, J. P. Cleveland, N. H. Thomson, P. K. Hansma, M. A. Wendman, G. Gurley, and V. Elings, "Short cantilevers for atomic force microscopy," *Review of Scientific Instruments*, vol. 67, no. 10, pp. 3583–3590, 1996.

[16] A. D. L. Humphris, M. J. Miles, and J. K. Hobbs, "A mechanical microscope: high-speed atomic force microscopy," *Applied Physics Letters*, vol. 86, pp. 034 106–1–034 106–3, 2005.

[17] M. J. Rost, L. Crama, P. Schakel, E. van Tol, G. B. E. M. van Velzen-Williams, C. F. Overgauw, H. ter Horst, H. Dekker, B. Okhuijsen, M. Seynen, A. Vijftigschild, P. Han, A. J. Katan, K. Schoots, R. Schumm, W. van Loo, T. H. Oosterkamp, and J. W. M. Frenken, "Scanning probe microscopes go video rate and beyond," *Review of Scientific Instruments*, vol. 76, no. 5, pp. 053 710(1–9), April 2005.

[18] L. M. Picco, L. Bozec, A. Ulcinas, D. J. Engledew, M. Antognozzi, M. Horton, and M. J. Miles, "Breaking the speed limit with atomic force microscopy," *Nanotechnology*, vol. 18, no. 4, pp. 044 030(1–4), January 2007.

[19] K. K. Leang and A. J. Fleming, "High-speed serial-kinematic AFM scanner: design and drive considerations," *Asian Journal of Control*, vol. 11, no. 2, pp. 144–153, March 2009.

[20] A. J. Fleming and S. O. R. Moheimani, "Sensorless vibration suppression and scan compensation for piezoelectric tube nanopositioners," *IEEE Transactions on Control Systems Technology*, vol. 14, no. 1, pp. 33–44, January 2006.

[21] A. J. Fleming and K. K. Leang, "Charge drives for scanning probe microscope positioning stages," *Ultramicroscopy*, vol. 108, no. 12, pp. 1551–1557, November 2008.

[22] A. J. Fleming and A. G. Wills, "Optimal periodic trajectories for band-limited systems," *IEEE Transactions on Control Systems Technology*, vol. 13, no. 3, pp. 552–562, May 2009.

[23] T. Ando, N. Kodera, T. Uchihashi, A. Miyagi, R. Nakakita, H. Yamashita, and K. Matada, "High-speed atomic force microscopy for capturing dynamic behavior of protein molecules at work," *e-Journal of Surface Science and Nanotechnology*, vol. 3, pp. 384–392, December 2005.

[24] T. Sulchek, S. C. Minne, J. D. Adams, D. A. Fletcher, A. Atalar, C. F. Quate, and D. M. Adderton, "Dual integrated actuators for extended range high speed atomic force microscopy," *Applied Physics Letters*, vol. 75, no. 11, pp. 1637–1639, 1999.

[25] Y. Jeong, G. R. Jayanth, and C.-H. Menq, "Control of tip-to-sample distance in atomic force microscopy: A dual-actuator tip-motion control scheme," *Review of Scientific Instruments*, vol. 78, no. 9, pp. 093 706(1–7), 2007.

[26] T. Akiyama, U. Staufer, and N. F. de Rooij, "Atomic force microscopy using an integrated comb-shape electrostatic actuator for high-speed feedback motion," *Applied Physics Letters*, vol. 76, no. 21, pp. 3139–3141, May 2000.

[27] J. Maess, A. J. Fleming, and F. Allgöwer, "Simulation of dynamics-coupling in piezoelectric tube scanners by reduced order finite element models," *Review of Scientific Instruments*, vol. 79, pp. 015 105(1–9), January 2008.

[28] C. J. Chen, "Electromechanical deflections of piezoelectric tubes with quartered electrodes." *Applied Physics Letters*, vol. 60, no. 1, pp. 132–134, January 1992.

[29] A. A. Mamun, I. Mareels, T. H. Lee, and A. Tay, "Dual stage actuator control in hard disk drive - a review," in *Proc. Annual Conference of the IEEE Industrial Electronics Society*, vol. 3, Roanoke, Virginia, November 2003, pp. 2132–2137.